Geosynchronous Environment for Severe Spacecraft Charging

M.S. Gussenhoven*
Boston College, Chestnut Hill, Massachusetts
and
E.G. Mullen†
Air Force Geophysics Laboratory, Hanscom Air Force Base, Massachusetts

A survey of data from the first year of the P78-2 (SCATHA) satellite operations showed that severe spacecraft frame charging (ϕ_f) both in sunlight (-340 V) and in eclipse (> -8 kV) occurred on 24 April 1979. Analysis of the data indicates that if the sunlight charging environment had been present during eclipse, the vehicle would have charged in excess of -15 kV, which is above any known charging level observed to date for the SCATHA satellite. Therefore, the environment at the peak of the sunlight charging at ~0650 UT 24 April 1979 was chosen for this "worst case" study. The environment at this time is characterized by an injection of high-energy (30-335 keV) electron fluxes whose combined current correlates with ϕ_f with a correlation coefficient of 0.95. The fluxes were highly anisotropic, maximizing perpendicular to the magnetic field. The low-energy (<4 keV) electron population had a density <1 cm^{-3} and the low-energy ions were near background. The measured electron distribution functions, when fitted to double Maxwellians by a least-squares technique, show that throughout the sunlight charging period the high and low temperatures remained nearly the same, while the density of the high-energy component followed the charging levels. The injection occurred simultaneously with the rapid return of the magnetospheric magnetic field to a more dipolelike configuration.

Introduction

WITH the launch of the geosynchronous satellite ATS-5 in 1969, and subsequent analysis of the particle data by DeForest,[1] the space physics and engineering communities have become increasingly concerned with the problem of spacecraft charging. A recent review of this field has been compiled by Garrett.[2] Additional specifics of recent work in the area can be found in the proceedings of five symposia.[3-7] In January 1979, the Spacecraft Charging AT High Altitudes (SCATHA) satellite P78-2 was launched as a joint USAF/NASA mission with the most complete instrumentation complement flown to date for the purpose of studying spacecraft charging effects at near-geosynchronous altitudes, and testing techniques for mitigating them.

Because spacecraft at geosynchronous orbit can charge to levels significant enough to impact and degrade system performance, there is a need for space vehicle design engineers to have a "worst case" charging environment. However, a definition of "worst case" has been somewhat elusive. Proposed definitions include: 1) the measured environment which produces the largest vehicle frame (ground) to plasma potential difference (ϕ_f); 2) the environment which produces the largest differential potential between adjacent spacecraft surface materials; 3) the highest density hot plasma environment encountered at geosynchronous orbit; and 4) the environment which causes the greatest number of satellite anomalies. In this study we discuss an environment that produced one of the largest satellite frame potentials on the SCATHA satellite in its first year of operation. The event occurred on 24 April 1979. The environment presented is also an extremely severe geosynchronous environment, having an exceptionally dense plasma population in the high-energy (>20 keV) range. This can be seen by comparing to statistical results from the ATS 5 and 6 satellites available in Ref. 8.

We do not specifically address here the question of when the highest levels of differential charging are found. An entire array of sample surfaces was monitored on SCATHA for just this purpose. Results of the differential charging during the period we report here may be found in Ref. 9. A statistical survey of the SCATHA differential charging results by Mizera and Boyd[10] indicate that the differential charging found on 24 April 1979 was in the highest 10% of occurrence. In addition, the study of differential charging during the spring of 1981 eclipse season[11] gives strong evidence that the worst differential charging occurs between a frame in sunlight or penumbral eclipse and shadowed insulators. Differential charging is greatly reduced when all surfaces are in shadow (umbral eclipse). These results support our attempt to define a worst environment for charging in terms of sunlit situations even though the frame potential (ϕ_f) in eclipse is generally higher by an order of magnitude.

Deep dielectric charging, which is produced by higher energy particles ($\sim >0.5$ MeV) and may be the principle cause of pulse-measured arcing, is probably unrelated to the surface charging discussed here. However, both types of charging can produce satellite anomalies. Results from the transient pulse monitor onboard SCATHA may be found in Ref. 12.

The "worst case" described here is a sunlight charging event, although the data extend into satellite eclipse. In eclipse, the satellite potential in this case, severely affects the ion and electron spectra inhibiting an accurate measurement of the ambient particles. In sunlight, the satellite potential is much smaller since photoelectrons provide a significant amount of the current balance, and the particle spectra are affected to a much lesser degree. Estimates of the satellite potential, had the vehicle been in eclipse when it encountered this "worst case" environment, exceed measured eclipse potentials.

Different spacecraft charge to different levels in the same environment depending on their surface materials, size, shape, and orientation to the sun. Therefore, absolute charging levels experienced on a particular satellite cannot be accurately compared to absolute charging levels on a satellite of different design. However, if an environment maximizes the relative charging on a space vehicle, then that environment may truly be a "worst case" environment. Below we present an example of such a charging environment as encountered by SCATHA on 24 April 1979. Comments are made on the environmental conditions and regimes where the highest level spacecraft charging can be expected.

Presented as Paper 82-0271 at the AIAA 20th Aerospace Sciences Meeting, Orlando, Fla., Jan. 11-14, 1982; submitted Jan. 22, 1982; revision received May 17, 1982.

*Senior Research Physicist, Physics Department.
†Physicist, Plasma, Particles, and Fields Branch.

Table 1 Experiments on the SCATHA satellite

Experiment no.	Experiment title
SC2	Sheath electric fields Electrons, ions 5 eV-18 keV
SC5	Rapid scan particle detector Electrons, ions 50 eV-1 MeV
SC8	Energetic ion composition E/q: 100 eV-32 keV
SC9	UCSD charged particle experiment Electrons, ions 1 eV-81 keV
SC10	Electric field detector
SC11	Magnetic field monitor

To orient those unfamiliar with the SCATHA satellite, we shall briefly describe the satellite and instrumentation. Geophysical conditions on the charging day are also discussed. The satellite plasma environment is described in terms of time and pitch angle variations of particle fluxes in different energy ranges, and in terms of magnetic field variations. Parameters that are related to satellite charging are identified and correlated. Finally, the particle measurements are represented in forms more suitable for modeling spacecraft charging and discussed in terms of their accuracy in reproducing the ambient plasma features. This should allow each reader to adapt the results to his particular needs.

Satellite Description and Instrumentation

The P78-2 (SCATHA) satellite is cylindrical in shape (~1.75 m in length and diameter) and has seven experimental booms. The satellite is spin-stabilized at approximately 1 rpm with the spin axis of the satellite in its orbital plane and normal to the Earth-sun line. This allows an outward pointing detector on the cylindrical surface to sample nearly all pitch angles. The satellite is in a 5.5×7.7 R_E ($R_E = 1$ Earth radius), low inclination (~8 deg) orbit and drifts eastward at about 6 deg per day. For a more detailed review of the satellite and its instrumentation, see Ref. 13.

Of the thirteen separate experimental payloads onboard the SCATHA satellite, data from six of the payloads are used in this paper. The six are referred to throughout the paper as SC2, SC5, SC8, SC9, SC10, and SC11. For convenient reference we identify each of the experiments in Table 1 with a brief summary of the detector capabilities of the particle experiments. Since the six experiments are well documented by Stevens and Vampola,[13] only a short description of the two payloads most critical to this study is given here. These experiments are the AFGL rapid scan particle detector (SC5) and the NASA/Goddard electric field detector (SC10).

The SC5 detector is comprised of two sets of spectrometers which allow a determination of the ion differential flux from ~50 eV to several MeV and the electron differential flux from ~50 eV to 1 MeV. One set of spectrometers is parallel to the spin axis and measures energetic particles at a nearly constant pitch angle. The other set of spectrometers is perpendicular to the spin axis and sweeps through nearly all pitch angles once per spin. Data for each energy range are obtained once per second; thus, this instrument provides very fast time resolution with rather broad energy resolution. Its pitch angle resolution is excellent for determing directions and anisotropies in particle flows to the satellite. A summary description and calibration of the instrument are given in Hanser et al.[14]

The SC10 detector consists of two 50-m antennas that form a 100-m dipole. The inner 30 m of each antenna is coated with Kapton insulation so that the outer 20-m conducting surfaces of copper beryllium act as a double floating probe ensemble to measure dc electric fields in the ambient plasma. The instrument also measures the voltage difference between one of the antennas and spacecraft ground. When the conducting tip floats at plasma potential, this mode of operation provides high time resolution (twice per second) measurements of ϕ_f. The materials and length of the boom should guarantee this to be the case in sunlight for satellite potentials less than ~1 keV, to within an accuracy of several volts. In addition, Mullen and Gussenhoven[15] have shown that the potentials measured by SC10 in sunlight are equivalent to those determined by the ion charging peaks in the SC9 data for potentials up to 800 V to within the resolution of SC10 and the spread in the SC9 measured ion peak. Thus, the SC10 data are used here primarily as a high time resolution sunlight vehicle charging monitor.

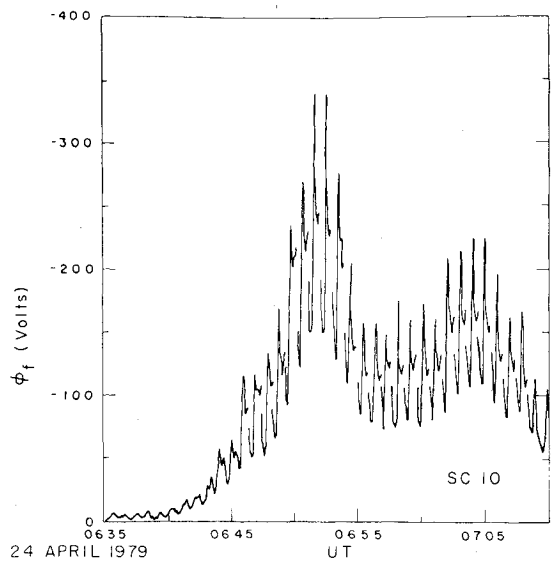

Fig. 1 Vehicle frame charging (ϕ_f) measured by SC10 at 0.5 s resolution for the pre-eclipse period.

"Worst Case" Spacecraft Charging Level

The "worst case" spacecraft charging levels occurred on SCATHA on 24 April 1979 between 0635 and 0730 UT. For this period the satellite varied in distance from the center of the Earth between 6.45-6.75 R_E (passing through geosynchronous orbit), in L-shell‡ from 7.0-7.3, and in magnetic latitude from 0.7-1.2°N. At ~0635 UT (~2300 local time), while still in sunlight, ϕ_f began to increase. It increased steadily (in the negative sense) from several volts to several hundred volts until a maximum sunlight value of −340 V was reached between 0651 and 0653 UT. Over the next 20 min the satellite potential had large variations, but remained charged above the ~ −50 V level until the satellite entered eclipse at 0710 UT. In eclipse, ion peaks in the SC5 and SC9 data show that the satellite potential reached a maximum value greater than −8 kV, and remained at potentials greater than −1 kV throughout the eclipse period. Upon re-entering sunlight at 0805 UT, ϕ_f dropped to less than ~ −50 V and returned to an uncharged state by 0850 UT.

While the eclipse condition resulted in an increase of the satellite potential by nearly two orders of magnitude, the worst environment for spacecraft charging actually occurred during the period of sunlight charging. Evidence for this is given below. In fact, the −340 V charging peak represents one of the highest levels of SCATHA sunlight charging observed during the first year of operation. The satellite potential, as measured by SC10, for the sunlight charging period (0635-0710 UT) is shown in Fig. 1. Here, every point

‡L-shells are surfaces generated by rotation of a dipole field about the magnetic axis. They are labeled by the distance in Earth radii that the field lines cross the magnetic equator.

(one per 0.5 s) is plotted, except for those times when the SC10 boom was pointing nearly directly at the sun, or was in the vehicle shadow. At these times, boom charging effects contaminate the data. The high time resolution of the SC10 measurement clearly shows a spin-cycle variation in the satellite potential superimposed on a more slowly varying response to environmental changes. Figure 2 is an expansion of the potential plot for three spin cycles, from 0655 to 0658 UT. The spin-cycle variation is nearly 80 V and is extremely regular. It is due to rotation of various satellite surface materials with different photoelectron emissivity properties and/or booms in and out of sunlight. SC10 charging events have been examined for 75 days under differing degrees of particle anisotropy, and the maximum and minimum spin-cycle charging levels are always at the same sun angle orientation independent of particle pitch angle, thus ruling out particle pitch angle as the causative factor for the spin-cycle variation. To determine temporal variations in ϕ_f independent of material properties, sun angle, and so on, we represent ϕ_f by its maximum value for each spin.

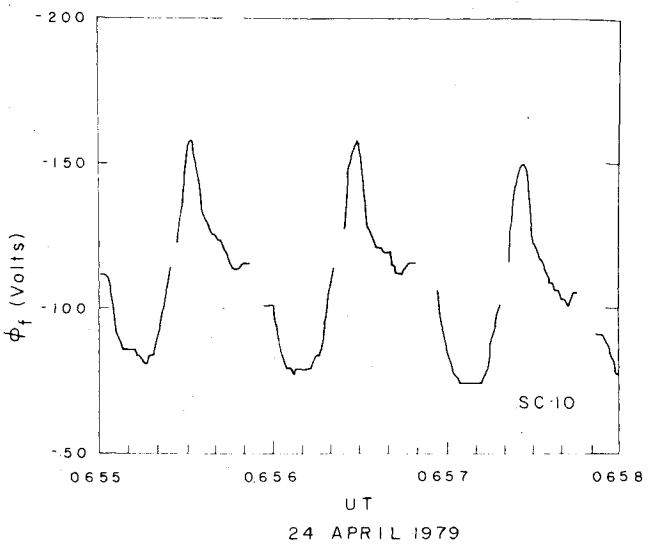

Fig. 2 Vehicle frame charging (ϕ_f) measured by SC10 at 0.5 s resolution, in an expanded time scale showing spin/sun angle effects.

Magnetospheric Conditions for "Worst Case" Event

The specific changes in the magnetic field and particle populations that produced the charging situation on 24 April 1979 are presented. First, however, it should be noted that the magnetic activity on 24 April, as measured at the Earth's surface, was significantly less than that of the previous three days. Following a gradual but sustained increase in activity on 21 April, the occurrence of multiple substorms was measured at high-latitude magnetometer stations through 23 April. Further, when the SCATHA satellite entered the plasma sheet in the midnight sector on 22 and 23 April, multiple dynamic injections were encountered. The magnetic field also showed large-scale variations from the model field and on 22 April was quite turbulent in nature. The substorm activity on 24 April was greatly reduced prior to 0600 UT. Although 22 April was the most active day, satellite charging in sunlight did not exceed -40 V, and in eclipse, -400 V. On 23 April sunlight charging was as high as -150 V, and -1.2 kV in eclipse.

Magnetospheric Magnetic Field

Onboard SCATHA the magnetic field, as measured by the SC11 NASA/Goddard magnetometer[16] has the following variations in solar magnetic coordinates§ (designated B_x, B_y, B_z) when compared to the quiet magnetic field model of Olson and Pfitzer.[17] For ~24 h prior to 0600 UT on 21 April, the measured and model fields were nearly identical. At ~ 0600 UT (2100 MLT) on 21 April, a gradual decrease in B_z of ~30 nT took place over 1 h. The B_x and B_y components varied only slightly during this time. This type of variation from the model, dipolelike field indicates a more taillike configuration. The field remained moderately disturbed and taillike through 1200 UT on 22 April, when it returned to the model field. A smaller, taillike excursion from the model field occurred at ~1600 UT on 22 April and persisted with variations to 0645 UT on 24 April. At this time, approximate values for the measured (model) field components were : $B_x = 7(5)$ nT; $B_y = -12(-3)$ nT; $B_z = 70(90)$ nT. By 0655 UT on 24 April, the magnetic field had dynamically returned to a near-model field configuration. The variations in B_z from 0635-0710 UT on 24 April are shown in detail in a later section.

Particle Populations

At ~0330 UT (~1900 MLT) the SCATHA satellite entered the plasma sheet. At this time the vehicle saw a sharp increase in low-energy (<1 keV) electrons.[18] As the satellite moved to higher altitudes it crossed more energetic Alfven layers (energy-dependent boundaries between the plasma sheet particles and zones of forbidden access which are dominated by the co-rotation electric field). This dispersion in electron fluxes, which is characteristic of a quiet plasma sheet crossing,[19] continued for several hours. At ~0630 UT, the satellite was well within the plasma sheet, having crossed the 20 keV Alfven layer. A major change occurred in the electron spectrum at ~0615 UT with sharp decreases in electron fluxes for energies less than 1 keV.

The particle fluxes, as measured by SC5, are shown in detail in Fig. 3. The left-hand side of Fig. 3 gives the electron fluxes for energies from 620 eV to 335 keV; the right-hand side gives ion fluxes for energies from 4 keV to 388 keV. The fluxes are plotted in linear scales. The solid lines represent measurements made perpendicular to the magnetic field. The dotted lines are for measurements made at pitch angles nearest to 180 deg (antiparallel to the magnetic field). For the period of interest, the closest approach to the field was ~15 deg. The crossings of Alfven layers for the 9 and 23 keV energy channels were at 0605 and 0635 UT, respectively. Lower-energy crossings occurred prior to 0530 UT. The fluxes are preferentially aligned perpendicular to the magnetic field indicating well-developed loss cones, a characteristic of the quiet plasma sheet.

After 0600 UT, perpendicular electrons with energies less than 5 keV began to decrease, approaching the flux levels of the parallel electrons. By 0635 UT the lower-energy particle population was nearly isotropic and remained this way through to 0900 UT.

At ~0645 UT the perpendicular electron fluxes in all the high-energy channels, down to and including the 23 keV channel, increased sharply. This was followed by a second, larger increase that peaked near 0651 UT. The increases occurred only in the perpendicular electrons resulting in a more anisotropic hot component in the plasma. This dynamic injection in the highest-energy channels is associated with the SCATHA "worst case" charging event and an isolated substorm seen in ground magnetic variations. After the injection peak, the electron fluxes and average energy decreased (with fluctuations) until 0900 UT, at which time the total electron environment was nearly isotropic. The ions over the energy range from ~4 keV to 388 keV are shown in the right-hand side of Fig. 3. This figure shows that 1) the >100 keV perpendicular ion fluxes had the same large-scale increase near 0650 UT that the electrons had; 2) the 23.1 keV perpendicular ions decreased markedly during the peak of the

§In solar magnetic coordinates the z axis is parallel to the north magnetic pole, the y axis is perpendicular to the Earth-sun line, and the x axis completes the Cartesian coordinate system and is positive in the sunward direction.

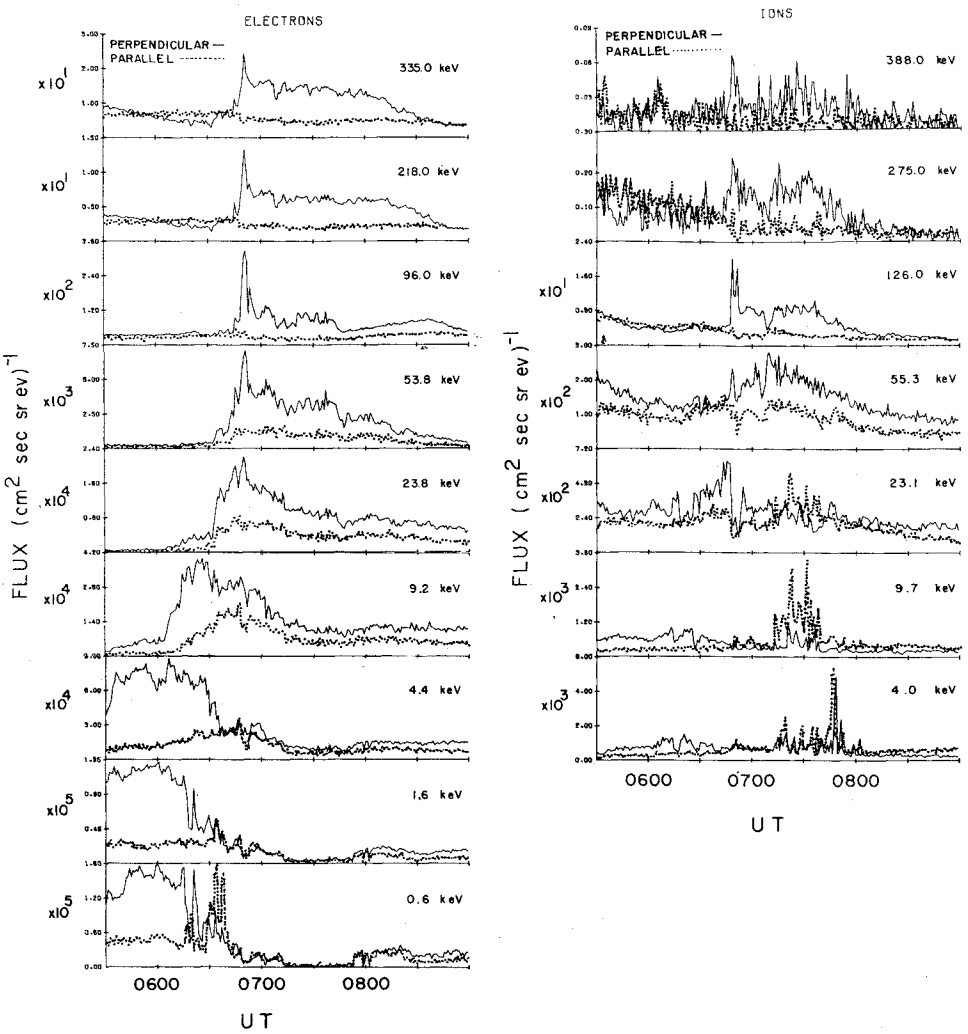

Fig. 3 SC5 electron (left) and ion (right) fluxes as measured perpendicular (solid line) and at ~165 deg (dashed line) to the magnetic field over the energy range 0.6-335 keV for electrons and 4-388 keV for ions plotted vs UT on 24 April 1979.

electron injection event after 0650; 3) the ions, accelerated to the vehicle during high-level charging in eclipse (0710-0800 UT), were preferentially field aligned; and 4) although the lower-energy ions were more isotropic over the entire period than their electron counterparts, the >100 keV ions behaved in the same way as the high-energy electrons. A 20 min average density ratio $n(0^+)/n(H^+)$ over the energy range measured (0.2-32.0 keV) was 0.41 ± 0.10 for the sunlight charging period.[20] Although ion mass data provided from the SC8 Lockheed ion mass spectrometer gave evidence for field-aligned streaming of 0^+ during high-level charging periods, no pitch angle information was available for this time period. SC5 measurements of ion fluxes for the energy range 50 eV-2 keV (not shown in Fig. 3), reach values above background only sporadically, last only 1-3 s, and fluctuate greatly. No significant changes in these fluxes are discernible from the precharging through the sunlight charging period. Ion counts in the SC2 detectors for the energy range 74-360 eV are low prior to sunlight charging and show weak field alignment. During sunlight charging low-intensity, field-aligned charging peaks can frequently, but not always, be identified. We concluded from these measurements that the low-energy (<1 keV) ion population was very small during the charging event. On 24 April, GEOS 2, in synchronous orbit and with the capability of measuring the cold ion population, lagged SCATHA by ~12 h in local time. No significant cold ion population (<1 cm^{-3}) was measured on either 23 or 24 April, in the midnight sector (2100-0300 MLT).[21]

The characteristics of the magnetospheric plasma for the "worst case" charging on SCATHA are summarized by the spectra in Fig. 4. The ion and electron distribution functions (density in six-dimensional phase space, measured in

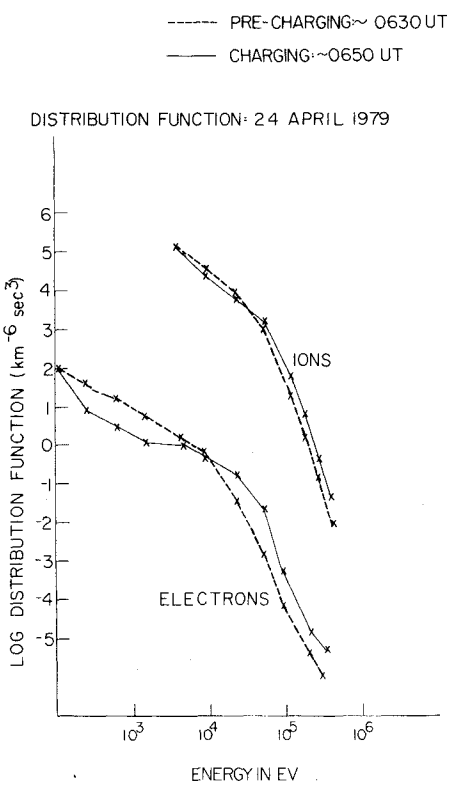

Fig. 4 Ion and electron distribution functions for precharging environment at ~0630 and a charging environment at ~0650 UT plotted vs particle energy on 24 April 1979.

$km^{-6}s^3$), for measurements made perpendicular to the magnetic field, are shown for the highest sunlight charging level at ~0650 UT (solid line); and for reference, for the precharging time, 0630 UT (dashed line).

The ion and electron spectra both deviate from the precharging spectra in the same manner; a decrease in phase space density for lower energies and an increase for higher energies. The energy at which no change occurs is 10 keV for electrons and 30 keV for ions. The electron distribution function variations are greater than those for ions. We note here that although the precharging spectra are used for reference, they themselves are considerably harder than those frequently found in the plasma sheet.

Data Analysis

In the previous section, evidence was presented which indicates that the "worst case" environment occurred during the injection of high-energy (> ~30 keV) electrons perpendicular to the magnetic field. An accompanying decrease in electrons with energies near 1 keV also occurred. In addition, the environment was characterized by the absence of a significant ($\leq$ 1 cm^{-3}) cold to low-energy ion population. In this section, a statistical analysis of the data shows that strong interrelationships exist among ϕ_f, high-energy electron fluxes, and magnetic field behavior. The moments of the particle distribution functions during charging are calculated and the distribution functions fit to double Maxwellians to give characteristic densities and temperatures for populations less than and greater than 4 keV. Together these studies present a picture of the high-level charging environment.

Correlation Analysis

Figure 5 shows in detail geophysical parameters whose variations are similar to the variations in ϕ_f for sunlight conditions. Similar agreements were also found for eclipse conditions. The bottom panel gives ϕ_f. The values of ϕ_f are obtained from SC10, taking the maximum value per spin. The second panel is the z component of the magnetospheric magnetic field in solar magnetic coordinates as measured by SC11. Also shown (dashed line) is the z component of the model magnetospheric field of Olson and Pfitzer.[17] The top two panels are electron fluxes for two energy ranges measured by SC5 and plotted once per spin when the detector was perpendicular to the magnetic field. The average energies for the two ranges are 53.8 and 96.0 keV. All variables are plotted linearly.

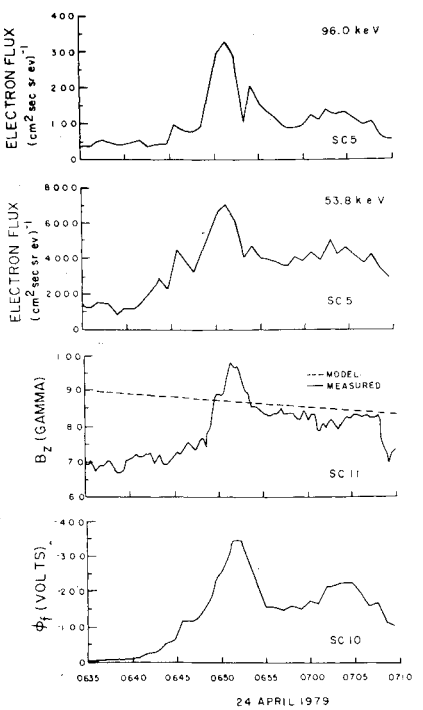

Fig. 5 A time history of vehicle frame charging in sunlight together with associated geophysical parameters between 0635 and 0730 UT on 24 April 1979. The top two panels show SC5 electron fluxes measured at 96 and 53.9 keV, respectively. The third panel shows the B_z component of the magnetic field in SM coordinates as measured by SC11 (solid line) and the Olson and Pfitzer quiet model for same interval (dashed line). The bottom panel shows ϕ_f as measured by SC10.

To make a quantitative assessment of the relationship between electron fluxes and ϕ_f, linear regressions between the two were performed for each energy channel above the charging peak. In sunlight, the regressions were performed for the period 0635-0710 UT. For each energy channel 37 pairs of points were used, one pair per spin. The resulting correlation coefficients, (r's) are given in Table 2. A Student's t test of the significance level of the coefficients shows that they are highly significant (exceed the 0.1% level) for all channels including and above the 53.8 keV channel. The correlation coefficient drops sharply from 0.94 to 0.42 between the 53.8 keV channel and the 23.8 keV channel. It reverses sign and remains low for the 9.2 and 4.4 keV channels. For the two lowest channels, 1.57 and 0.62 keV, there is a high anticorrelation between the fluxes and ϕ_f. Similar correlations of ϕ_f, as measured by SC9, and electron flux in eclipse showed the same trend, although the coefficients themselves were not quite as high.

Because of the high correlation between charging and high-energy fluxes, we conclude that it is the high-energy tail of the electron spectrum that is primarily responsible for high-level satellite charging. The high correlation coefficients also permit extrapolation of the fluxes in sunlight on 24 April 1979 to give eclipse values for ϕ_f. To do this, the assumption must be made that the low-energy component (electron and ion) of the plasma remained approximately constant from 0635 to 0730 UT. The assumption is reasonable since the satellite remained in the plasma sheet for the entire period, and there was no significant cold ion population (see previous section). Extrapolating ϕ_f to eclipse conditions using linear regression equations calculated during eclipse for both the 96 keV and the 53.8 keV electron fluxes gives values of 18 and 15 kV, respectively, at 0651 UT. Both values are higher than any known charging level seen to date on the SCATHA satellite.

The lower-energy fluxes also contribute to the charging level, although it is in an anticorrelative way as can be seen in Table 2. Surfaces with high secondary and backscatter coefficients (> ~1.5) over the low-energy portion of the spectrum (~100 eV to 2 keV) return more electrons to the ambient than are incident from the ambient in this energy range. Thus the net current in this range is a discharging current, as opposed to the charging current of the higher-energy electrons. Reducing the discharging current by reducing the incident electron current < 4 keV, thus, contributes to the satellite charging.

Table 2 Correlation coefficients of ϕ_f vs electron flux in sunlight

SC5 energy bin (keV)	r
0.62	−0.87
1.57	−0.72
4.4	−0.28
9.2	−0.36
23.8	0.42
53.8	0.94
96	0.85
218	0.92
335	0.92

The B_z component of the magnetic field is also seen to vary considerably over the period 0630-0730 UT. The largest variations were between 0648 and 0653, simultaneous with the injection events (Fig. 5). B_z was found to correlate highly with both the SC10 charging levels prior to eclipse ($r=0.93$) and the 53.8 keV electron fluxes ($r=0.90$) through the entire period. This interrelationship among B_z, ϕ_f, and high-energy electron flux provides insight into physical mechanisms that occur in the plasma sheet during high-level charging events. Sufficient SCATHA data have been examined to indicate that the return of the B_z to a more dipolar configuration is directly related to the high-energy particle injection process near geosynchronous orbit. A complete description of the mechanisms of injection events remains one of the outstanding problems of space physics and is certainly beyond the scope of this paper.

Moments of the Distribution Function

Certain properties of the plasma can be calculated by taking various velocity moments of the ion and electron distribution functions constructed from particle measurements. For SC5, the first four moments (zero- through third-order) are related to number densities and fluxes of a given particle species as follows:

Number density (cm^{-3}), n:

$$\int f d^3v \; ; \tag{1}$$

Number flux ($cm^{-2}s^{-1}$), NF:

$$\int |v| f d^3v \; ; \tag{2}$$

Energy density (eV-cm^{-3}), ϵ:

$$1/2\, m \int v^2 f\, d^3v \; ; \tag{3}$$

Energy flux (eV-$cm^{-2}s^{-1}$), EF:

$$1/2\, m \int |v^3| f d^3v \tag{4}$$

In these equations, f and m are the distribution function and mass for a given particle species, and the integration is taken over the entire velocity space. For the SC5 measurements, symmetry is assumed in the plasma perpendicular to the magnetic field and integrations are performed over pitch angle and v. The fluxes (number and energy) in Eqs. (2) and (4) are the total fluxes that would be intercepted by an infinitesimally small, omnidirectional receiving device. Average directional fluxes can be calculated from Eqs. (2) and (4) by multiplying by $1/4\pi$. In practice, directional fluxes (no integration in angular space) are often used to obtain pitch angle information.

From the first four moments there are two ways of defining temperature:

$$T_{avg} = \frac{2}{3} \cdot \frac{\epsilon}{n}, \tag{5}$$

and

$$T_{rms} = \frac{1}{2} \cdot \frac{EF}{NF} \tag{6}$$

For a distribution function that is well fit by the Maxwell-Boltzmann function:

$$f(v) = n\left(\frac{m}{2\pi kT}\right)^{3/2} e^{-mv^2/2kT} \tag{7}$$

the two temperatures are equal; that is,

$$T = T_{rms} = T_{avg} \tag{8}$$

(In Eq. (7), k is the Boltzmann constant $= 1.38 \times 10^{-6}$ erg/K.) In general, however, distribution functions are not Maxwellian over the entire energy range and the concept of temperature is an ambiguous one.

Table 3 gives the first four moments of the ion and electron distribution functions, together with T_{avg} and T_{rms}, during the "worst case" charging at ~0650 UT on 24 April. We average the values obtained over the four spins of peak charging (6:50-6:53 UT) to reduce effects of scatter. The SC5 measurements over the energy range 100 eV-400 keV were used to construct the distribution functions. Integrations over pitch angle were used for all moments; therefore, the number and energy flux are average directional quantities. The moments for ions were calculated assuming hydrogen as the only species. R.G. Johnson[20] has provided composition data in the 0.2 to 32 keV energy range that show that the average density ratio $n(0^+)/n(H^+)$ is between ~0.3 and 0.5 over the daylight charging period. This would have the effect of raising the ion number density and energy density roughly by a factor of 2. The temperatures and fluxes would remain the same. Care must be taken in interpreting the moment results since the cold population was missing and the low-energy end of the spectrum was influenced by ϕ_f.

The same moments assuming isotropic particle distributions and using particles fluxes at a 90 deg pitch angle are given in Table 4. The difference between the corresponding quantities in Tables 3 and 4 gives a measure of the anisotropy of the plasma.

A Two-Maxwellian Description of the "Worst Case" Environment

The technique of using a double Maxwellian to fit the actual distribution function does not necessarily guarantee the best mathematical fit; however, the double Maxwellian is easy to use (only four numbers are required to define a distribution function) and is conceptually and computationally understood by the engineering community. The one requirement that must be imposed on any representation chosen for the actual distribution function is that it not obscure the physical process it models.

A method of determining double Maxwellian densities and temperatures for a distribution function is least-squares fitting the logarithm of the distribution function to energy over specific energy ranges. Visual inspection of individual distributions for SC5 data was used to determine an ap-

Table 3 Moments and temperatures integrated over pitch angle

		Electrons	Ions
n,	cm^{-3}	0.9	2.3
NF,	$cm^{-2}-s^{-1}$	4.7×10^{9}	2.0×10^{8}
ϵ,	$eV-cm^{-3}$	9.6×10^{3}	1.7×10^{4}
EF,	$eV-cm^{-1}-s^{-1}$	8.4×10^{13}	4.9×10^{12}
T_{avg},	keV	7.7	5.5
T_{rms},	keV	9.0	13

Table 4 Moments and temperatures using ⊥ particles only

		Electrons	Ions
n,	cm^{-3}	1.1	2.3
NF,	$cm^{-2}-s^{-1}$	7.8×10^{9}	2.1×10^{8}
ϵ,	$eV-cm^{-3}$	1.8×10^{4}	2.4×10^{4}
EF,	$eV-cm^{-1}-s^{-1}$	1.7×10^{14}	6.8×10^{12}
T_{avg},	keV	9.6	8.1
T_{rms},	keV	10.6	15.0

propriate energy range for calculating the high-energy Maxwellian characterized by n_2 and T_2. The energy range selected for both ions and electrons was 4-400 keV. The low-energy parameters n_1 and T_1 were calculated by fitting to all the residual data below 4 keV after subtracting extrapolated values from the high-energy fit. Figure 6 shows values of the distribution functions for ions and electrons measured by SC5 at ~0650 UT on 24 April. Measurements made both perpendicular and near-parallel to the magnetic field are given. Also shown is the two-Maxwellian representation of each distribution. Solid (dashed) lines represent distributions perpendicular (parallel) to the magnetic field. The low-energy Maxwellians (to ~4 keV) must be regarded with caution for the following reasons: 1) the low-energy measurements did not extend below 100 eV; 2) the low-energy particles were affected by the satellite potential and corrections to the distribution function have not been made for this effect; and 3) the low-energy ions were near background and varied sporadically. To create a time-varying, two-Maxwellian description of the charging period, a method of extrapolating through noisy data was developed which resulted in placing too much weight on values just above background. This is evident in Fig. 6 where a low-energy Maxwellian has been included although there is only one good lower-energy ion data point at this time.

The high-energy Maxwellians for both ions and electrons, and for both parallel and perpendicular directions to the magnetic field, deviate from the actual distribution functions in two ways, neither of which prevents them from appropriately representing the charging process: first, they underestimate the lower-energy spectrum (from ~2-10 keV), which has been shown to anticorrelate with satellite charging at the lower end; and second, they overestimate the values in the energy range (20-200 keV) where direct correlation with charging was found. Thus, in each case the discrepancies between the Maxwellian fit and the actual spectrum place additional emphasis on the particle population that drives satellite charging. The electron and ion densities and temperatures that characterize the double Maxwellians in Fig. 6 are listed in Table 5. These represent distribution functions at the time of the sunlight charging peak. While Table 5 provides two sets of double Maxwellians—one set perpendicular and one set parallel to the local magnetic field—it is clear that using the perpendicular values for the electrons maximizes the high-energy component and minimizes the low-energy component which have been found to correlate and anticorrelate with the charging level, respectively. Thus, using perpendicular electron values only gives an even more extreme charging environment than the actual one. On the other hand, for ions reduction of the low-energy ion population worsens the charging situation, and consequently use of the parallel Maxwellians provides the extreme ion description. These considerations may be useful in attempts to reproduce a "worst case" charging environment in the laboratory.

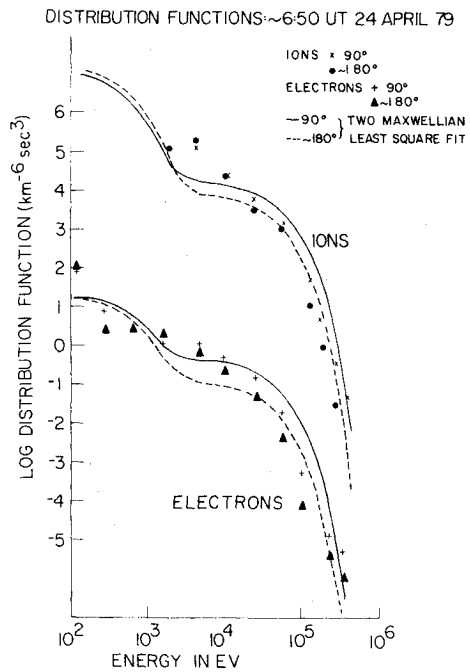

Fig. 6 Ion and electron distribution functions perpendicular and approximately antiparallel to the magnetic field together with their two Maxwellian least-square fits for the "worst case" charging environment on 24 April 1979. The distribution functions are plotted vs energy from 100 eV to 400 keV.

The variations in the four components (n_1, n_2, T_1, and T_2) for electrons with pitch angles ~75 deg are shown in Fig. 7 for the period from 0530 UT to 0730 UT. T_2, although relatively high, varies only slightly over the entire period; T_1 varies considerably. The high-energy electron density, n_2, rises steadily over the interval from 0530 UT to ~0651 UT when it peaks. On the other hand, n_1 maximizes near 0614 UT, at which time it begins a gradual but variable decline until about 0714 UT. The total electron density (n_1 plus n_2) varies between approximately 1 and 2 particles/cm^3 over the entire period, with n_1 noticeably suppressed due to the high negative vehicle potential after eclipse entry at 0710 UT. (No attempt was made to correct the spectra for charging effects.)

Figure 7 graphically portrays the results of the earlier statistical studies; that is, that the high-energy electron current or density is the driver in charging spacecraft to high levels. The decrease (anticorrelation) of n_1 near 0651 UT and the n_2 increase suggest that the low-energy particles are being accelerated to higher energies during injection events, and that the introduction of a new higher-energy population is not necessarily required. The high- and low-energy ion densities remain nearly constant, each between 1 and 2 particles/cm^3 during the entire period. The high-energy ion temperature stays near 28 keV, and the low-energy temperature near 300 eV. (Again, caution is advised in using the low-energy values.)

Discussion

Spacecraft charging results from conservation of current to and from a space vehicle. The satellite potential (ϕ_f) varies until current balance is attained. For a satellite in the magnetospheric environment, this relationship may be written:

$$J_E(\phi_f) - [J_I(\phi_f) + J_{SE}(\phi_f) + J_{SI}(\phi_f) + J_{BSE}(\phi_f) + J_{PH}(\phi_f)] = 0; \quad (9)$$

where:

J_E = ambient electron current at the spacecraft surface
J_I = ambient ion current at the spacecraft surface
J_{SE} = secondary emitted electron current due to ambient electrons
J_{SI} = secondary emitted electron current due to ambient ions

Table 5 Worst case least-squares particle environment fit (~0650 UT 24 April 79)

	n_1, cm^{-3}	n_2, cm^{-3}	T_1, keV	T_2, keV
Ions				
⊥	0.6	1.3	0.2	28.0
∥	1.6	0.6	0.5	29.5
Electrons				
⊥	0.2	1.2	0.4	27.5
∥	0.1	0.8	0.5	27.8

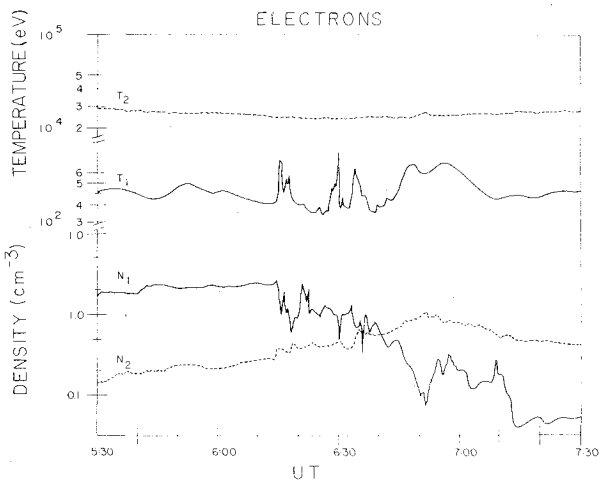

Fig. 7 Two Maxwellian electron temperatures T_1 and T_2 and densities n_1 and n_2, calculated by least-squares fitting the distribution functions, plotted vs UT for the period from 0530 to 0730 UT 24 April 1979.

J_{BSE} = backscattered emitted electron current due to ambient electrons
J_{PH} = photoelectron current

Here we use the convention that electron currents to the satellite are positive.

At geosynchronous (or near-geosynchronous) orbit, a satellite is usually in one of two very different plasma regimes; the plasmasphere or the plasma sheet. The plasmasphere has as its source the ionosphere and is a cold (several eV), dense ($\sim$10-100 cm^{-3}) plasma that corotates with the Earth and extends out from the ionosphere. The outer boundary of the plasmasphere varies greatly with magnetic activity and local time. In quiet periods it can extend beyond geosynchronous orbit, particularly in the dusk and premidnight sectors. The outer boundary of the plasmasphere is not always well defined, and clouds or bursts of cold plasma can extend outward into the neighboring region of the plasma sheet.

The plasma sheet begins where corotation effects are dominated by the cross-tail magnetospheric electric field. In some local time sectors the outer boundary of the plasmasphere and the inner boundary of the plasma sheet are identical. In others they are separated by a region referred to as the trough. The source of the plasma sheet is unclear, although there is evidence that both solar wind and ionospheric particles are variably involved. Acceleration mechanisms are required to transform both populations into the hot plasmas observed in the plasma sheet. Densities in the plasma sheet are typically of order 1 cm^{-3} and temperatures of the high-energy component typically exceed 10 keV, for both ions and electrons. Thus, although the density in the plasma sheet is low, the ambient currents are not. High-level space vehicle charging is limited to periods when the vehicle is in the plasma sheet.

The plasma sheet expands and contracts with solar and magnetic activity. It can reach inward to less than 5.5 R_E during high activity periods. After several magnetically quiet days (days of low K_p), the inner edge of the plasma sheet can be out beyond geosynchronous orbit, in which case no significant spacecraft charging effects would be observed. The boundary of the plasma sheet in local time at geosynchronous orbit can range from $\sim$12 h around local midnight to none at all. Within the plasma sheet, there exist periods when rapid Earthward movements or energetic particles are observed. These particle injections appear in the midnight sector in conjunction with geomagnetic substorms and high latitude auroral activity, and depending on their energy and density can create satellite charging. The cold (<1 to 100 eV) particle density in this region is typically low and often less than 1 cm^{-3}. It is this combination of intense high-energy electron fluxes in the near absence of a cold ion population that is responsible for high-level spacecraft charging.

Numerous papers have been written that try to explain the mechanism for injection events in the plasma sheet. Here we do not try to develop or justify any model, but try only to give a cursory explanation of the data in terms of current thinking. Sauvaud and Winckler[22] give a schematic representation of the geomagnetic field lines during the different phases of a substorm. A substorm, as described in their paper, consists of an expansion phase when the magnetic field lines move out and become more taillike and a collapse phase when the field lines return to a more dipolar configuration. As can be seen in Fig. 5, it is during periods when the magnetic field collapses from a more tailward configuration toward a more dipolar configuration that electrons are accelerated to and/or injected at higher energies. These large magnetic field collapses are associated with substorm onsets which can be seen on the ground as increases in the auroral electrojet index AE. During substorm collapse, the high-energy electron densities can be sufficiently large in certain spatial regimes of the plasma sheet to cause large current imbalance to satellites in the same regime. Numerous substorms take place that would severely charge space vehicles if the spacecraft were 1) in eclipse; 2) in the plasma sheet with large high-energy ($>\sim$30 keV) electron density; 3) in a plasma sheet with little or no cold plasma population; and 4) oriented in such a way that large areas were exposed perpendicular to the magnetic field. Although the eclipse case is the extreme for frame charging, it is not necessarily the extreme for differential charging. Luckily, however, the probability of a satellite being at the right place at the right time under the right conditions to experience a "worst case" environment is quite small. Also, the exact position in local time where the injection front first reaches geosynchronous altitude is not clear. Further statistical studies of the SCATHA data base should provide insight into locating this region.

The environment observed at $\sim$0650 UT on 24 April 1979, and called here a "worst case" environment, occurred in an injection event associated with an isolated substorm observed in ground magnetograms after a long active period (multiple substorms). The electron fluxes associated with charging as shown in Fig. 3 were very anisotropic, with the highest fluxes being perpendicular to the field lines. As was also determined in Table 2 and shown in Fig. 5, the particles that directly correlate with ϕ_f are the particles in the 53.8 keV energy range and above. Summing the currents in the 53.8 through 335 keV energy channels and performing a linear regression with ϕ_f gives a correlation coefficient of 0.95. This indicates that it is the total current for energies above $\sim$30 keV (given the ΔE of the 53.8 keV channel) that is driving ϕ_f negative. (See, for example, Garrett et al.[23]) The lower energy fluxes (and currents), although larger, evidently produce enough backscatter and secondary electrons to balance themselves minus the photoelectron current. Evidence for high secondary yields for lower-energy particles was given by Sternglass.[24] An attempt to take advantage of materials with high secondary emission coefficients to influence spacecraft design to reduce charging was proposed by Rubin et al.[25]

Conclusion

The environment observed at $\sim$0650 UT on 24 April 1979 has been shown to be a severe charging environment that could produce detrimental effects on different space systems. Spacecraft perform a wide range of functions, and how those functions can be degraded depends heavily on the energy range, anisotropy, and composition of the particles to which they are most susceptible. Here we have examined an environment which produced one of the highest level sunlight and eclipse charging (ϕ_f) events observed during the first year

of SCATHA operations. The ϕ_f in and of itself is not damaging to space systems, but the differential charging associated with it can be. Various environmental parameters have been shown to be highly correlated with ϕ_f. Although the environment described above will seldom be encounterd over a vehicle's lifetime, it is representative of the type of environment that can seriously degrade system performance at geosynchronous orbit. It is recognized that SCATHA has yet to experience a superstorm that might change current thinking on the limit of plasma sheet particle populations. However, until such time as that data might become available, 24 April 1979 – 0650 UT is a good example of a "worst case" environment.

Acknowledgments

Many people have contributed to this effort without whose inputs this report could not have been written. For those staff members at the various contract organizations who work in the shadows and whose names do not appear, a heartfelt thanks. The authors would also like to thank the SCATHA experimenters: D.A. Hardy, AFGL: T.L. Aggson, NASA/Goddard; B.G. Ledley, NASA/Goddard; E.C. Whipple, UCSD; P.E. Mizera, Aerospace; J.F. Fennell, Aerospace; R.G. Johnson, Lockheed; J.B. Reagan, Lockheed; H.C. Koons, Aerospace; and R.C. Adamo, SRI for use of their data and the countless discussions of its interpretation. A special thanks to D.E. Delorey of Boston College who endured numerous computer program modifications to give us a quality product, and to his contract monitor, R.E. McInerney of AFGL who provided us with the necessary computer resources to accomplish the task. Thanks also to N. Heinemann of Boston College for data presentations, L. Cassidy of Regis College for graphics and artwork, and J. Cronin of AFGL for his computer graphics and statistical analysis. The work of M.S. Gussenhoven was supported by the Air Force Geophysics Laboratory under Contract F19628-79-C-0031.

References

[1] DeForest, S.E., "Spacecraft Charging at Synchronous Orbit," *Journal of Geophysical Research*, Vol. 77, 1972, pp. 651-659.

[2] Garrett, H.B., "The Charging of Spacecraft Surfaces," *Reviews of Geophysics and Space Physics*, Vol. 19, 1981, pp. 577-616.

[3] Rosen, A., ed., *Spacecraft Charging by Magnetospheric Plasma*, Progress in Astronautics and Aeronautics, Vol. 47, AIAA, New York, 1976.

[4] Pike, C.P. and Lovell, R.R., eds., *Proceedings of the Spacecraft Charging Technology Conference*, AFGL-TR-77-0051/NASA TMX-73537, 1977.

[5] Finke, R.C. and Pike, C.P., eds., *Spacecraft Charging Technology-1978*, NASA CP-2071/AFGL-TR-79-0082, 1979. Technology-1980, NASA CP-2182/AFGL-TR-81-0270, 1981.

[6] Stevens, M.J. and Pike, C.P., eds., *Spacecraft Charging.*

[7] Tasca, D.M., ed., *IEEE Annual Conference on Nuclear and Space Radiation Effects, Trans. Nuclear Science*, Vol. NS-28, 1981.

[8] Garrett, H.B., "Review of Quantitative Models of the 0- to 100-keV Near-Earth Plasma," *Reviews of Geophysics and Space Physics*, Vol. 17, 1979, pp. 397-417.

[9] Mizera, P.F. et al., "First Results of Material Charging in the Space Environment," *Applied Physics Letters*, Vol. 37, 1980, pp. 276-279.

[10] Mizera, P.F. and Boyd, G.M., "A Summary of Spacecraft Charging Results," submitted to *Journal of Spacecraft and Rockets*, 1982.

[11] Mizera, P.F., Fennel, J.F., Koons, H.C., Vampola, A.L., and Hall, D.F., "Spacecraft Charging in the Spring of 1981," Aerospace Corporation, El Segundo, Calif., TOR-0181(6508-05)-1, Sept. 1981.

[12] Adamo, R.C. and Matarrese, J.R., "Transient Pulse Monitor (TPM) Data from the SCATHA/P78-2 Spacecraft," submitted to *Journal of Spacecraft and Rockets*, 1982.

[13] Stevens, J.R. and Vampola, A.L., eds., "Description of the Space Test Program P78-2 Spacecraft and Payloads," SAMSO-TR-78-24, 1978.

[14] Hanser, F.A., Hardy D.A., and Sellers, B., "Calibration of the Rapid Scan Particle Detector Mounted in the SCATHA Satellite," AFGL-TR-79-0167, 1979.

[15] Mullen, E.G. and Gussenhoven, M.S., "High Level Spacecraft Charging Environments Near Geosynchronous Orbit," AFGL-TR-82-00639, 1981.

[16] Ledley, B.V., private communication, 1981.

[17] Olson, W.P. and Pfitzer, K.A., "A Quantitative Model of the Magnetospheric Magnetic Field," *Journal of Geophysical Research*, Vol. 79, 1974, pp. 3739-3748.

[18] Fennell, J.F., private communication, 1981.

[19] Kivelson, M.G., Kaye, S.M., and Southwood, D.J., "The Physics of Plasma Injection Events," in *Dynamics of the Magnetosphere*, D. Reidel, Hingham, Maine, 1979, pp. 385-394.

[20] Johnson, R.G., private communication, 1981.

[21] Wrenn, G., private communication, 1981.

[22] Sauvaud, J.-A. and Winckler, J.R., "Dynamics of Plasma Energetic Particles, and Fields Near Synchronous Orbit in the Nighttime Sector During Magnetospheric Substorms," *Journal of Geophysical Research*, Vol. 85, 1980, pp. 2043-2056.

[23] Garrett, H.B., Schwank, D.C., Higbie, P.R., and Baker, D.N., "Comparison Between the 30 to 80-keV Electron Channels on ATS 6 and 1976-059A During Conjunction and Application to Spacecraft Charging Prediction," *Journal of Geophysical Research*, Vol. 85, 1980, pp. 1155-1162.

[24] Sternglass, E.J., "Secondary Electron Emission and Atomic Shell Structure," *Physical Review*, Vol. 80, 1950, pp. 925-926.

[25] Rubin, A.G., Rothwell P.L., and Yates, G.K., "Reduction of Spacecraft Charging Using Highly Emissive Surface Materials," in *Effects of the Ionosphere on Space and Terrestrial Systems*, John M. Goodman, U.S. Government Printing Office, Wash., D.C., 1978, pp. 313-316.